INVESTIGATION OF THE OPTICAL PROPERTIES OF InSb THIN FILMS GROWN ON GaAs BY TEMPERATURE-DEPENDENT SPECTROSCOPIC ELLIPSOMETRY

Yuanlan Liang [1], Fangze Wang [1], Xuguang Luo [1], Qingxuan Li [1], Tao Lin [1], Ian T. Ferguson [2], Qingyi Yang [1], Lingyu Wan [1], Zhe Chuan Feng [1*]

[1] *College of Physics Science & Technology, Guangxi University, Nanning 530004, China; e-mail: fengzc@gxu.edu.com; taolin@gxu.edu.cn*
[2] *Missouri University of Science & Technology, Rolla, MO 65409, USA*

InSb thin films were grown on GaAs substrates by metal organic chemical vapor deposition (MOCVD) and investigated by temperature-dependent spectroscopic ellipsometry (TD-SE). The refractive index, extinction coefficient, and dielectric function of the InSb films were extracted. The variation of critical point energies (E_1, $E_1+\Delta_1$, E_2, E_1') related to the excited state transitions of InSb and the second energy derivatives of the dielectric function at different temperatures showed that the InSb thin film had high electrical and optical stability at the evaluated temperatures. TD-SE analysis revealed a temperature range suitable for the use of InSb/GaAs-based devices. Beyond 250°C, InSb was heavily oxidized to form a thin In-O layer, causing a pronounced change in the optical constants. The results indicated that optimized InSb thin films grown on GaAs by MOCVD possess good optical and structural properties.

Keywords: *InSb thin film, spectroscopic ellipsometry, refractive index, extinction coefficient, dielectric function.*

ИССЛЕДОВАНИЕ ОПТИЧЕСКИХ СВОЙСТВ ТОНКИХ ПЛЕНОК InSb, ВЫРАЩЕННЫХ НА ПОДЛОЖКАХ GaAs, МЕТОДОМ ТЕМПЕРАТУРНО-ЗАВИСИМОЙ СПЕКТРОСКОПИЧЕСКОЙ ЭЛЛИПСОМЕТРИИ

Y. Liang [1], F. Wang [1], X. Luo [1], Q. Li [1], T. Lin [1], I. T. Ferguson [2], Q. Yang [1], L. Wan [1], Z. C. Feng [1*]

УДК 543.42;539.216.2

[1] *Физико-технический колледж, Университет Гуанси, Наньнин, 530004, Китай; e-mail: fengzc@gxu.edu.com; taolin@gxu.edu.cn*
[2] *Миссурийский университет науки и технологии, Ролла, MO 65409, США*

(Поступила 15 января 2018)

Тонкие пленки InSb выращены на подложках GaAs методом химического осаждения из газовой фазы путем термического разложения и исследованы с помощью температурно-зависимой спектроскопической эллипсометрии (TD-SE). Найдены показатель преломления, коэффициент экстинкции и диэлектрическая проницаемость пленок InSb. Изменение энергий критических точек (E_1, $E_1 + \Delta_1$, E_2, E_1'), связанное с переходами InSb в возбужденном состоянии, и вторых производных диэлектрической функции по энергии при разных температурах показывает, что тонкая пленка InSb обладает высокой стабильностью электрических и оптических свойств в исследуемом температурном диапазоне. Анализ TD-SE позволил установить область температур для использования устройств на основе InSb/GaAs. Выше 250°C InSb интенсивно окисляется, образуя тонкий слой In-O, вызывающий значительное изменение оптических констант. Показано, что оптимизированные тонкие пленки InSb, выращенные на подложках GaAs, обладают хорошими оптическими и структурными свойствами.

Ключевые слова: *тонкая пленка InSb, спектроскопическая эллипсометрия, показатель преломления, экстинкция, диэлектрическая проницаемость.*

Introduction. Crystalline indium antimonide (InSb) possesses a narrow bandgap of 0.18 eV at room temperature (RT) and the highest electron and hole mobility of 7.8×10^4 $cm^2/V\cdot s$ among III–V group compound semiconductors. This is very useful for a number of applications, for example, in high-speed electronic devices, mid-infrared photodetectors, and high-performance magnetoresistive sensors [1–10]. The InSb/GaAs heterojunction structure is widely used in high-performance InSb-based infrared (IR) detectors, despite a large lattice mismatch of about 14.6% between InSb and GaAs [2, 11, 12]. Metal organic chemical vapor deposition (MOCVD) has been developed as a viable technology to produce large-scale InSb thin films on the GaAs substrate. Techniques have been developed to overcome the difficulty of the large lattice mismatch between film and substrate for large-scale industrial IR optoelectronics and automobile applications [13–15]. InSb-based devices have theoretically been shown to have the potential for high performance over a wide temperature range [1]. Therefore, it is necessary to experimentally study their temperature-dependent optical properties, including refractive index (n), extinction coefficient (k), and dielectric function (ε) in the range 300–600 K for infrared applications without liquid nitrogen cooling and high-power-density devices.

There have been a few experimental studies of the optical properties of bulk and epitaxial InSb [5, 16–22]. Miyazaki et al. reported the $\varepsilon(E)$ spectra of InSb epitaxial films with different substrate temperatures and various depositions [16]. Tae Jung Kim et al. reported the critical points (CPs) of bulk InSb in the temperature range 31–675 K by analyzing the dielectric function data obtained from spectroscopic ellipsometry (SE) measurements, and the blue shift and sharpening of the CPs structures were observed [17–19]. D'Costa et al. investigated the optical properties of InSb films on the GaAs substrate compared to the InSb bulk crystal using SE at RT [20]. Haruyuki Sano et al. performed *ab initio* calculations of the InSb characteristics and analyzed the differences of the optical properties of the crystalline and liquid states [21]. E. B. Elkenany et al. studied the temperature effect (0–500 K) on the optoelectronic properties of the InSb semiconductor using the local empirical pseudo-potential method [22]. Muhammad Hilal et al. investigated the electro-optical properties of InSb under the influence of spin-orbit interaction at RT [5]. However, the optical properties of InSb films grown on GaAs for a wide temperature range have not been reported.

In this work, SE was used as a nondestructive technique, with good precision in a wide spectral region, to examine the film thickness, optical constants, and microstructures of InSb/GaAs heterostructures. The optical properties of InSb thin films grown on GaAs substrates were studied by SE in the temperature range RT–300°C, i.e., 573 K. The changes in Ψ and Δ were measured and subsequently used to extract the refractive index (n), extinction coefficient (k), and dielectric function, related to the carrier concentration and mobility of InSb. Furthermore, to investigate the temperature dependence of the dielectric function, some critical parameters obtained from the SE results were also elucidated. The obtained results indicated that, despite a lattice mismatch of ~14.6% with the GaAs substrate, these InSb thin films on GaAs substrates have good optoelectronic properties in comparison with the bulk crystal after optimizing the control parameters during the MOCVD growth. Furthermore, our temperature-dependent spectroscopic ellipsometry (TD-SE) measurements and simulation revealed the formation of an indium-oxide thin layer, causing a large change in the optical constants.

Experimental. Crystalline InSb thin films grown on GaAs (100) substrates were prepared by the MOCVD method. Trimethylindium (TMIn) and trimethylantimony (TMSb) were used as In and Sb sources, respectively. The pressures of the indium and antimony bubblers were 429 and 323 Torr, respectively. The indium and antimony bubble flows were in the range 130–270 sccm. Hydrogen acted as the carrier gas and its flows were varied from 320 to 775 sccm. The rates of growth were between 0.65 and 1.2 μm/h, with the best growth rate at about 0.95 μm/h. The temperature growth was monitored by a single wavelength low-temperature pyrometer and fixed at 395°C. These growth processes resulted in thin film surfaces with excellent morphology, free of indium droplets. A typical InSb/GaAs sample was studied extensively in this paper. A number of measurements were performed for this epitaxial InSb sample, including investigation of the AFM surface morphology and RF sheet resistivity. Herein we present the results of Hall measurements, scanning electron microscopy (SEM), etc. [23].

Results and discussion. A dual rotating-compensator Mueller matrix ellipsometer (ME-L ellipsometer, Wuhan Eoptics Technology Co. Ltd., China), equipped with a Linkam Scientific heating and cooling stage device (THMSG600E), was used for the acquisition of the ellipsometric spectra of InSb thin films. Two parameters Ψ and Δ, determining the amplitude ratio and phase difference between the light waves, respectively, can be extracted from the ellipsometric data as a function of wavelength λ from 193 to 1700 nm at 1 nm step or energy E from 0.73 to 6.43 eV. The SE spectra of bulk InSb and InSb thin films studied here are shown in Fig. 1. Their spectral oscillations are similar, which indicates similar optical parameters like n or k.

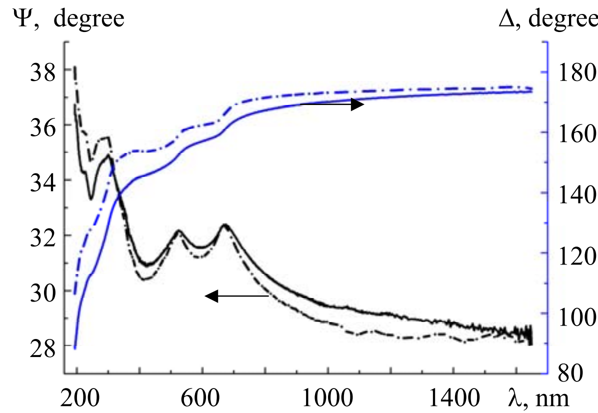

Fig. 1. The SE spectra of bulk InSb (solid lines) and the InSb thin film grown on GaAs (dot-dash lines).

The Eomtrics software was applied to fit the SE data, as described below. The *n*, *k,* and ε at different temperatures (25–300°C) were derived through analysis of the SE data of this InSb sample. The complex dielectric function ε of InSb versus photon energy (*E*) was modeled using multiple Tauc–Lorentz oscillators. The Tauc–Lorentz model can be expressed as [24–26]:

$$\varepsilon_2(E) = \begin{cases} \dfrac{AE_0C(E-E_g)^2}{(E^2-E_0^2)^2+C^2E^2}\dfrac{1}{E}, & E > E_g, \\ 0, & E \le E_g, \end{cases} \tag{1}$$

where ε_2 is the imaginary part of the dielectric function and *E* is the photon transition energy. The values *A* and *C* are obtained by fitting Ψ and Δ. Equation (1) is useful for evaluating ε (or *n*, *k*). The real part of the dielectric function ε_1 is obtained by exploiting the Kramers–Kronig integrations, i.e.

$$\varepsilon_1(E) = \varepsilon_1(\infty) + \frac{2}{\pi}P\int_{E_g}^{\infty}\frac{\xi\varepsilon_2(\xi)}{\xi^2-E^2}d\xi\,, \tag{2}$$

where the term *P* is the main part of the Cauchy integral, where $\varepsilon_1(\infty)$ is added as a fitting parameter.

Assuming that the samples were heated by the ambient environment during testing, a structural model for bulk InSb and InSb thin films used for fitting the data was designed, including a surface roughness layer with 50% of air and 50% of the In_2O_3 material, an oxide layer of In_2O_3 and a crystalline InSb layer on the GaAs substrate. Then the measured data were simulated by the Bruggemen equivalent medium approximation model [27] according to the above structure. The SE fitting results of the InSb thin film at variable angles (50°, 55°, and 60°) are displayed in Fig. 2. The measured data were in good agreement with the model fit in the full spectral region. It is found that both Ψ and Δ changed with the incident angle. Therefore, all of the Ψ and Δ data with variable angles were considered in the calculation of the optical parameters of *n* and *k*. The obtained thickness of the InSb layer was 38.77 nm, which indicated the possibility of crystalline distortion and compressive stress induced by the lattice mismatch between InSb and GaAs in the InSb layer. Therefore, its optical properties may be different from the thick one or the bulk counterpart, and these differences become significant if the growth parameters are not optimized and the crystalline quality is low.

The fitting results showed that the obtained thickness of In_2O_3 layers in the major temperature range (25–250°C) was very small. For example, the obtained thickness of In_2O_3 layers for 250°C was less than 0.01 nm, while the value was 38.8 nm for the InSb layer; 0.01 nm is much thinner than one monatomic layer, so this indicates that oxide layers are unnecessary in the fitting structure models of these samples. Surprisingly, the sample for 300°C showed a 5.4 nm thickness for In_2O_3 and a 37.2 nm thickness for InSb. This indicates that the oxide layer cannot be ignored in the sample heated at 300°C. The obtained optical parameters like the refractive index and the extinction coefficient relating only to the InSb layers were extracted and analyzed below.

Figure 3 shows the similarity of the data of our work (solid lines) and the results from [28]. The refractive index of bulk InSb is greater than that of the InSb thin film in the wavelength range 200–725 nm, and the extinction coefficient of bulk InSb is larger than that of the InSb thin film in the range 315–1650 nm.

Figure 4 shows the variation of *n* and *k* of the InSb film from 25 to 300°C. As is seen, the InSb thin film contains several absorption peaks in the wavelength range 200–800 nm. They gradually and smoothly shift toward the longer wavelength region (red shift) and broaden with increasing temperature from RT to 250°C. However, as the temperature increases beyond 250°C up to 300°C, pronounced spectral variations occur. These variations are irreversible and permanent, even after repeating the SE tests by cooling the sample. This phenomenon implies that oxidation exerts a remarkable influence at 300°C, and our model cannot perfectly simulate the real structure. For example, an intermediate layer with a gradient oxygen concentration cannot be well simulated by the SE database. However, this result may be predicated on the high temperature limitation for the use of InSb/GaAs materials in ambient conditions.

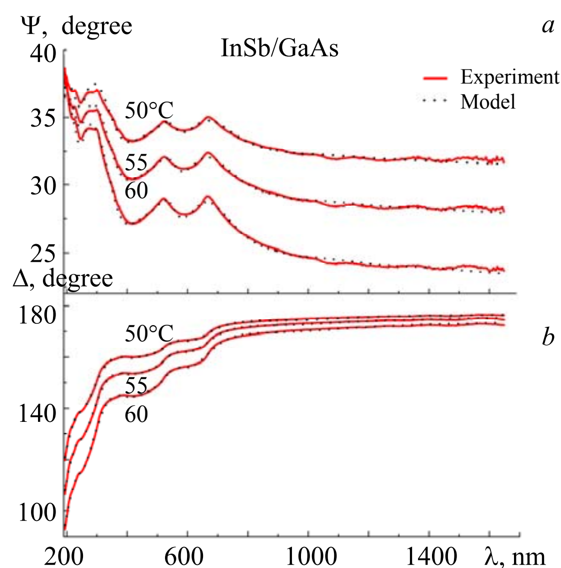

Fig. 2. The values of Ψ (a) and Δ (b) of the InSb thin film at different angles.

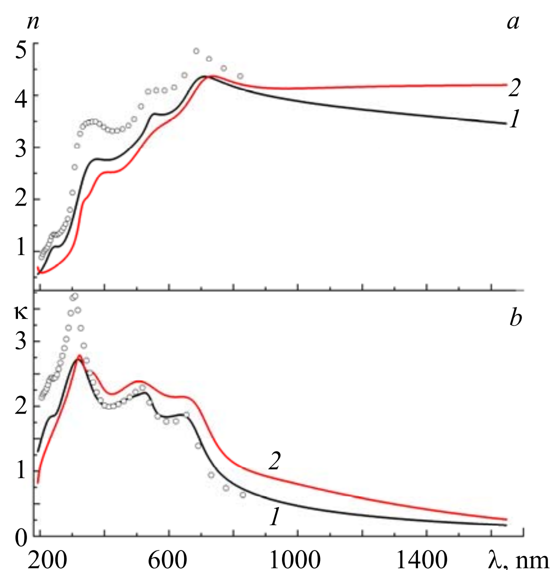

Fig. 3. The refraction index *n* (a) and the extinction coefficient *k* (b) of the InSb film (1) and bulk InSb (2) samples at RT. The circles are data from [28].

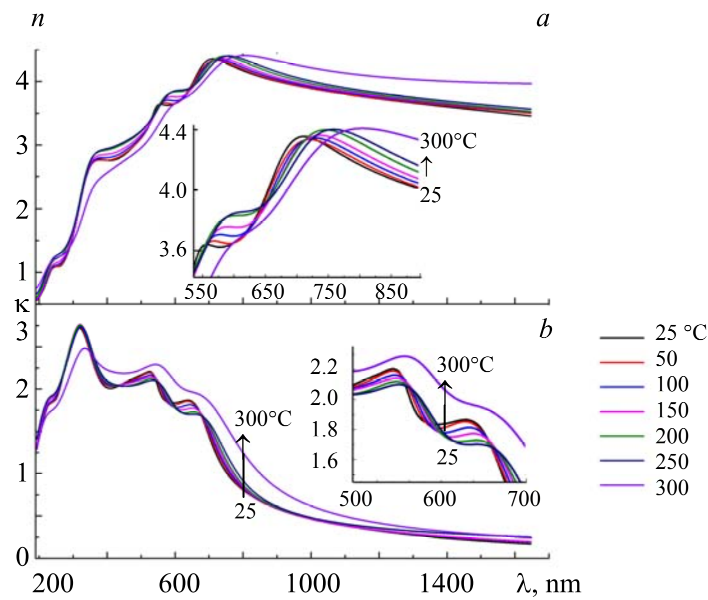

Fig. 4. The refraction index n (a) and the extinction coefficient k (b) of the InSb thin film as a function of the temperature.

The results of ε_1 and ε_2 of the InSb thin film at different temperatures are shown in Fig. 5. The properties of ε_1 and ε_2 in the wavelength range 200–800 nm are related to interband transitions because InSb has a narrow band gap of 0.18 eV. The high-energy region much beyond the bottom of the conduction band and related to electron-phonon interaction is critically dependent on the crystalline quality. Therefore, it is necessary to check these characteristics in detail at various temperatures.

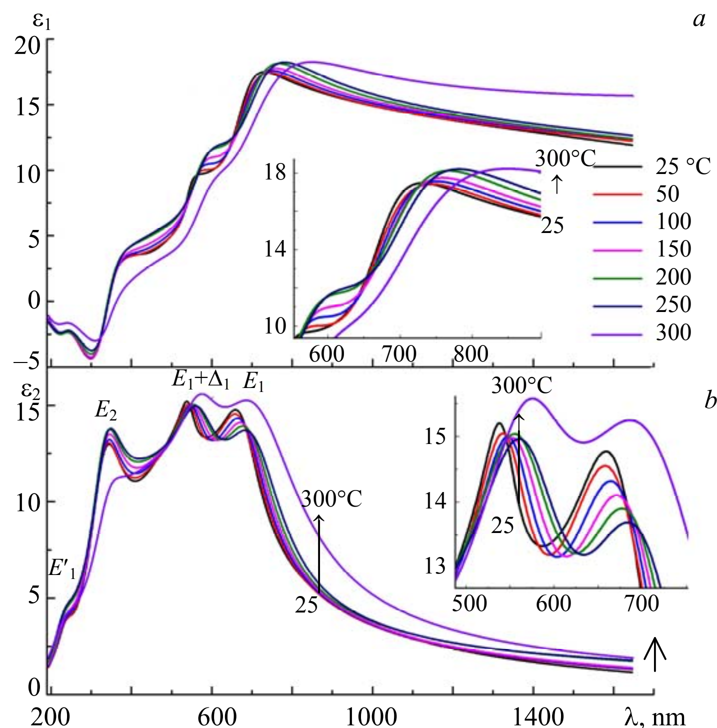

Fig. 5. The real (a) and imaginary (b) parts of the dielectric function ε of the InSb thin film as a function of the temperature.

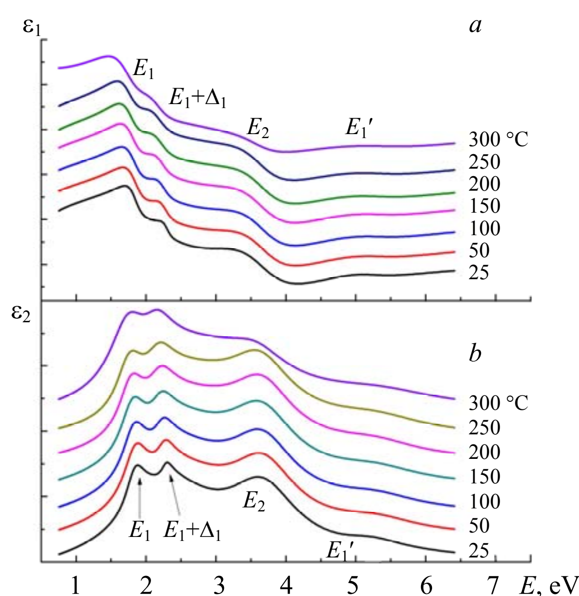

Fig. 6. The dielectric function ε of the InSb thin film at different temperatures.

The dielectric function ε of the InSb thin film at different temperatures as a function of the photon energy is shown in Fig. 6. The peaks in these spectra reflect the high-energy state transitions of the InSb thin film and can be used to obtain several critical energy points (E_1, $E_1+\Delta_1$, E_2, E_1'). The study of the changes of CPs energies at high temperatures is important for devices functioning at high temperature or output power.

The second energy derivatives of the dielectric function were investigated at different temperatures in order to distinguish the overlapping CP bands [29], as shown in Fig. 7. The solid lines and the dash lines are $d^2\varepsilon_1/dE^2$ and $d^2\varepsilon_2/dE^2$, respectively. Several selected spectra with temperature points of 25, 100, 200, and 300°C are displayed in Fig. 7. The sharp second-order peaks at 1.7–1.85 and 2.1–2.3 eV related to the energy levels E_1 and $E_1+\Delta_1$ can now be clearly seen. It can be clearly seen that the CPs move to the low energy side and the band structure becomes broader with increasing temperature, which indicates that both the transition probability and the carrier mobility decrease with temperature variation from RT to 300°C. Figure 8 shows the temperature dependences of the CPs E_1 and $E_1+\Delta_1$, which display a similar behavior as compared with the data of [19]. A red shift of the CPs is observed with increasing temperature as a result of the increased lattice constant and electron-phonon interaction [18, 19]. This demonstrates that the InSb thin film on GaAs has characteristics analogous to as bulk InSb. The structure of the peak related to the CPs can still be observed at 300°C from our experimental results. This indicates that this MOCVD-grown InSb material possesses high stability with increasing operational temperature.

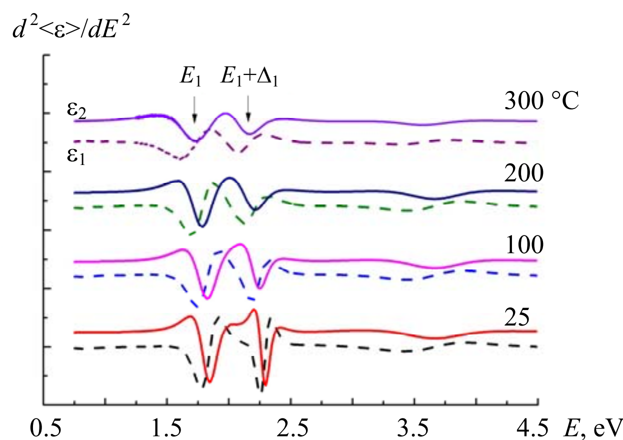

Fig. 7. The second energy derivatives of ε for temperatures from 25 to 300°C.

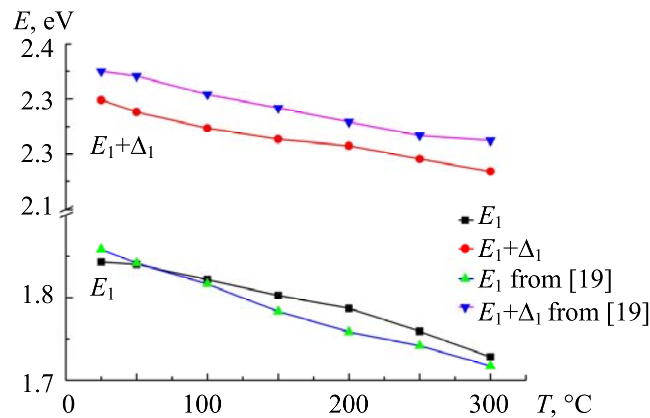

Fig. 8. The temperature dependences of E_1 and $E_1+\Delta_1$ CPs energies.
The pink and blue lines are results [19].

Conclusion. The optical properties of the InSb film grown on GaAs (100) by MOCVD were studied using SE at variable temperatures (25–300°C). The InSb SE data were analyzed by Tauc–Lorentz multiple oscillator modes. The variations of the refractive index (n), extinction coefficient (k), and dielectric function (ε) of the InSb thin film were extracted by analyzing the experimental SE data. It has been found that the absorption peaks shifted toward the longer wavelengths with increasing temperature. The second energy derivatives of the dielectric function were analyzed to get the temperature behavior of the critical parameters. This showed that the InSb epitaxial material under investigation had high electrical and optical stability at elevated temperatures. These results indicate that, despite a large lattice mismatch of ~14.6% for the InSb crystal on the GaAs substrate, the use of the MOCVD method with optimal growth conditions permits one to obtain thin film samples possessing optoelectronic properties comparable to their bulk counterpart. This work has revealed that a pronounced spectral variation, i.e., a large change in the optical or/and structural properties, occurred in the InSb film at temperatures beyond 250°C up to 300°C. This is caused by irreversible oxidation under ambient conditions at higher temperatures. However, the optical parameters of the InSb film vary gradually and smoothly with the temperature from RT to 250°C. This gives the opportunity to determine a temperature range for the application of InSb/GaAs-based devices. These results will be critical for designing high-performance InSb infrared optical thin film devices in the future.

Acknowledgment. We acknowledge financial support from the National Natural Science Foundation of China (Nos. 61367004 and 61504030) and special funding for Guangxi distinguished professors (Bagui Rencai and Bagui Xuezhe).

REFERENCES

1. V. K. Dixit, B. V. Rodrigues, H. L. Bhat, *J. Appl. Phys.*, **90**, 1750–1753 (2001).
2. V. K. Dixit, B. V. Rodrigues, H. L. Bhat, R. Venkataraghavan, K. S. Chandrasekaran, B. M. Arora, *J. Cryst. Growth*, **235**, 154–160 (2002).
3. T. D. Mishima**,** M. B.Santos, *J. Vac. Sci. Technol. B*, **B**, 1472–1474 (2004).
4. M. Shafa, H. Ji, L. Gao, P. Yu, Q. H. Ding, Z. H. Zhou, H. D. Li, X. B. Niu, J. Wu, Z. M. Wang, *Mater. Lett.*, **169**, 77–81 (2016).
5. M. Hilal, B. Rashid, S. H. Khan, A. Khan, *Mater. Chem. Phys.*, **184**, 41–48 (2016).
6. P. Ciochon´, N. Olszowska, S. Wróbel, J. Kołodziej, *Appl. Surf. Sci.*, **400**, 154–161 (2017).
7. Y. Contreras, A. J. Muscat, *Appl. Surf. Sci.*, **370**, 67–75 (2016).
8. I. D. Burlakova, K. O. Boltara, P. V. Vlasova, A. A. Lopukhina, A. I. Toropovd, K. S. Zhuravlevd, V. V. Fadeev, *J. Commun. Technol. Electron.*, **62**, 309–313 (2017).
9. A. V. Filatov, E. V. Susov, V. V. Karpov, V. A. Zhilkin, S. P. Ljubchenko, N. S. Kusnezov, A. V. Marushchenko, *J. Commun. Technol. Electron.*, **62**, 326–330 (2017).
10. V. Pusino, C. Z. Xie, A. Khalid, I. G. Thayne, D. R. S. Cumming, *Microelectron. Eng.*, **153**, 11–14 (2016).
11. T. Miyazaki, M. Kunugi, Y. Kitamura, S. Adachi, *Thin Solid Films*, **28**, 51–56 (1996).

12. K. Li, A. T. S. Wee, J. Lin, K. K. Lee, F. Watt, K. L. Tan, Z. C. Feng, J. B. Webb, *Thin Solid Films*, **302**, 111–115 (1997).
13. Y. Iwamura, N. Watanabe, *J. Cryst. Growth*, **124**, 371–376 (1992).
14. Z. C. Feng, C. Beckham, P. Schumaker, *Mater. Res. Soc. Symp. Proc.*, **450**, 450 (1997).
15. M. A. Mckee, B.-S. Yoo, R. A. Stall, *J. Cryst. Growth*, **124**, 286–291 (1992).
16. M. Razeghi, *EPJAP*, **23**, 149–205 (2003).
17. T. J. Kim, S. Y. Hwang, J. Choi, J. S. Byun, M. S. Diware, H. G. Park, Y. D. Kim, *J. Korean Phys. Soc.*, **61**, 439–443 (2012).
18. T. J. Kim, S. Y. Hwang, J. S. Byun, M. S. Diware, J. Choi, H. G. Park, Y. D. Kim, *J. Appl. Phys.*, **114**, 103501 (2013).
19. T. J. Kim, J. S. Byun, J. Choi, H. G. Park, Y. R. Kang, J. C. Park, Y. D. Kim, *J. Korean Phys. Soc.*, **64**, 1872–1877 (2014).
20. V. R. D'Costa, K. H. Tan, B. W. Jia, S. F. Yoon, Y. C. Yeo, *J. Appl. Phys.*, **117**, 223106 (2015).
21. H. Sano, G. Mizutani, *AIP Adv.*, **5**, 117110 (2015).
22. E. B. Elkenany, *Silicon*, **8**, 391–396 (2016).
23. T. R. Yang, Y. Cheng, J. B. Wang, Z. C. Feng, *Thin Solid Films*, **498**, 158–162 (2006).
24. G. E. Jellison Jr, F. A. Modine, *Appl. Phys. Lett.*, **69**, 371 (1996).
25. S. Chen, Q. X. Li, I. Ferguson, T. Lin, L. Y. Wan, Z. C. Feng, L. Zhu, Z. Z. Ye, *Appl. Surf. Sci.*, **421**, 383–388 (2017).
26. D. Xie, Z. R. Qiu, Y. Liu, D. N. Talwar, L. Y. Wan, X. Zhang, T. Mei, I. T. Ferguson, Z. C. Feng, *Mater. Res. Express*, **4**, 025903 (2017).
27. H. Fujiwara, *Spectroscopic Ellipsometry: Principles and Applications*, John Wiley & Sons, 181–184 (2007).
28. D. E. Aspnes, A. A. Studna, *Phys. Rev. B*, **27**, 985 (1983).
29. T. J. Kim, J. J. Yoon, S. Y. Hwang, D. E. Aspnes, Y. D. Kim, H. J. Kim, Y. C. Chang, J. D. Song, *Appl. Phys. Lett.*, **95**, 11902 (2009).